Journal of Systems Engineering and Electronics
Vol. 28, No. 3, June 2017, pp.481 – 492

Clutter suppression for hypersonic vehicle-borne radar with frequency diverse array

Xuzi Wu, Zheng Liu*, and Rong Xie

National Key Laboratory of Radar Signal Processing, Xidian University, Xi'an 710071, China

Abstract: The seriously range-ambiguous clutter is one of the main problems in clutter suppression for hypersonic vehicle-borne forward-looking radar. An approach based on the frequency diverse array (FDA) technique is proposed to mitigate the range-ambiguous clutter. The frequency increment is designed to distinguish the clutter at ambiguous ranges and suppress the clutter by using a subspace projection algorithm. On the platform with high altitude or limited array antennas, the proposed method performs better for its independence of the elevation degrees-of-freedom (DOF). Finally, simulation results verify the effectiveness of the proposed method.

Keywords: hypersonic vehicle, forward-looking array radar, clutter suppression, frequency diverse array.

DOI: 10.21629/JSEE.2017.03.08

1. Introduction

Hypersonic vehicle usually travels in the near space from 20 km to 100 km at a velocity greater than Mach 5. Owing to enormous potential in military and civilian application, it has drawn worldwide attention in recent decades [1,2]. One of its main tasks is acting as the weapon platform for rapid reconnaissance and precision guidance of missile on the ground/air moving targets. To realize this, the forward-looking array radar plays an important role in ground moving target indication (GMTI). However, the seriously expanded clutter Doppler brings a great challenge to GMTI on the hypersonic platform.

The space-time adaptive processing (STAP) technique has been known as an effective approach to suppress the Doppler spread clutter in the combination of angle and Doppler domains [3]. It relies on estimating the statistical characteristics of the ground clutter by the independent and identically distributed (IID) secondary range samples. In a forward-looking case, the clutter spectrum varies with the range, which is referred to as the range-dependence of the clutter [4]. It violates the IID condition, leading to the degradation in the accuracy of the covariance matrix and the STAP performance. Furthermore, due to the high platform altitude and velocity, it is difficult to choose a pulse repetition frequency (PRF) to ensure the clutter to be unambiguous in both the range and Doppler dimension [5]. One of the challenges for hypersonic vehicle-borne radar is the seriously range-ambiguous and range-dependent clutter that would be considered in this paper. So far, many methods have been proposed for compensating the range-dependence in forward-looking array radar [6 – 9], such as the Doppler warping (DW) method and the derivative based updating (DBU) method. Unfortunately, these methods can only be applied to the unambiguous range case. To circumvent this, the range-ambiguous clutter must be mitigated before the range-dependence compensation.

Recently, an exploitation of diversity in frequency domain, referred to as frequency diverse array (FDA), has attracted considerable attention [10 – 12]. Different from the well-known orthogonal frequency division multiplexing (OFDM) technique and multiple-input multiple-output (MIMO) array, FDA is not expected to exploit the diverse information to improve the overall performance since only a small frequency increment is used across the array elements and the frequency response is always assumed to be the same due to the negligible difference in the wavelengths [13]. It has been demonstrated to generate a range-dependent beampattern and inherently provide an increased degree-of-freedom (DOF) and additional capability in various processing systems [14 – 19]. In [14,15], the FDA was employed in the phased-array radar to synthetize the subarray and flexible transmit beampattern to enhance the range and angle estimation performance. The authors in [16,17] applied the FDA for high-resolution synthetic aperture radar (SAR) imaging. In electronic countermeasure scenarios, the FDA was used to suppress false tar-

Manuscript received March 08, 2016.
*Corresponding author.
This work was supported by the National Natural Science Foundation of China (61301282).

gets [18]. Reference [19] verified the ability of the FDA to suppress the range-ambiguous clutter in forward-looking airborne radar. However, the design of the FDA parameters and the seriously range-ambiguous clutter suppression were not considered in [19].

This paper proposes a new strategy of clutter suppression for hypersonic vehicle-borne radar. The key idea is to utilize the range-dependent characteristic of the FDA to distinguish the range-ambiguous clutter. Our main contributions include: (i) Under the consideration of a planar array, the models of the FDA beampattern and STAP signal are constructed, based on which new characteristics of the FDA are analyzed. It is found that the FDA changes the mainlobe clutter Doppler at different ranges and makes the clutter space-time spectrum shift along spatial dimension. To distinguish the range-ambiguous clutter, the constraint on the frequency increment is designed. (ii) The method for range-ambiguous clutter mitigation based on the subspace projection technique is developed. Although the problem has been considered in [20–23], we solve it by a new scheme based on the characteristics of the FDA. Unlike the methods that depend on the elevation DOF, the proposed method is independent of that. Therefore, it is superior in the situations where the number of range ambiguities is large or the antenna size on the platform is strictly limited.

The remaining sections are organized as follows. Section 2 gives an introduction to the FDA and presents the STAP signal model of the FDA radar. In Section 3, we analyze the new characteristics of the FDA beampattern and clutter space-time spectrum, based on which the design principles of the FDA are established. Next, we propose a clutter suppression approach in Section 4. Simulation examples and results are provided in Section 5. Finally, conclusions are drawn in Section 6.

2. Signal model

2.1 FDA preliminaries

The geometry of the forward-looking FDA radar system is shown in Fig. 1, where an (x, y, z) coordinate system is constructed. Ignore the vibration of the platform, radar travels along the ideal trajectory (standed in the positive x-direction) at a constant velocity v. H is the platform altitude above the earth. φ, θ and ψ are the azimuth angle, the elevation angle and the cone angle, respectively. Define $\boldsymbol{u}(\varphi,\theta) = [\cos\theta\cos\varphi, \cos\theta\sin\varphi, -\sin\theta]^{\mathrm{T}}$ as the spatial unit vector, where $(\cdot)^{\mathrm{T}}$ denotes the transpose operator. Without loss of generality, an $(M \times N)$-element rectangular array with uniform spacing d is considered. Taking the first element located at point $\mathrm{A}(0, 0, H)$ as the reference element, the relative location of the (m, n)th element is denoted by $\boldsymbol{d}_{m,n} = [0, (n-1)d, (m-1)d]^{\mathrm{T}}$. In this FDA radar, a small frequency increment is used across the horizontal elements, the signal transmitted by the (m, n)th element can be expressed as

$$s_{m,n}(t) = \exp(\mathrm{j}2\pi f_{m,n} t) \tag{1}$$

where $f_{m,n}$ denotes the radiated frequency as

$$f_{m,n} = f_0 + (n-1)\Delta f \tag{2}$$

where f_0 is the carrier frequency and Δf is the frequency increment which is negligible compared to f_0.

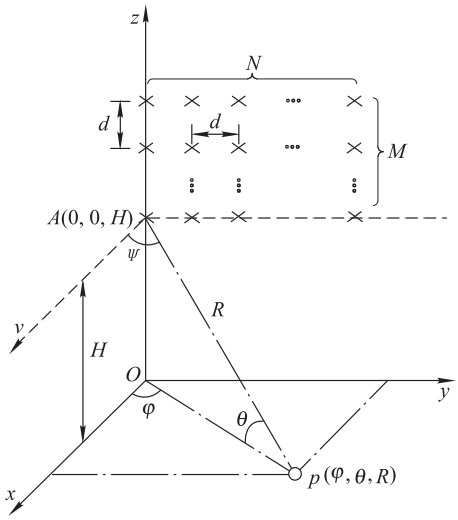

Fig. 1 Forward-looking FDA radar geometry

Considering a far-field point $p(\varphi,\theta,R)$ with R being the slant range to the reference element, the range to the (m, n)th element can then be expressed as

$$R_{m,n} = R - \boldsymbol{d}_{m,n}^{\mathrm{H}}\boldsymbol{u}(\varphi,\theta) = R - (n-1)d\cos\theta\sin\varphi + (m-1)d\sin\theta \tag{3}$$

where $(\cdot)^{\mathrm{H}}$ denotes the conjugate transpose operator.

In the receive chain, the reflected signals are filtered with $s_{m,n}$ in the (m, n)th element, remaining the signal with the frequency $f_{m,n}$. As a consequence, the signal received by the (m, n)th element can be expressed as

$$\begin{aligned} r_{m,n}(t,\varphi,\theta,R) = {} & \exp[\mathrm{j}2\pi f_{m,n}(t - 2R_{m,n}/c)] = \\ & \exp[\mathrm{j}2\pi f_{m,n} t - \mathrm{j}4\pi R/\lambda_0]\cdot \\ & \exp[\mathrm{j}4\pi(n-1)d\cos\theta\sin\varphi/\lambda_0]\cdot \\ & \exp[-\mathrm{j}4\pi(n-1)\Delta f R/c]\cdot \\ & \exp(-\mathrm{j}4\pi(m-1)d\sin\theta/\lambda_0)\cdot \\ & \exp[\mathrm{j}4\pi(n-1)^2\Delta f d\cos\theta\sin\varphi/c]\cdot \\ & \exp[-\mathrm{j}4\pi(n-1)(m-1)\Delta f d\sin\theta/c] \end{aligned} \tag{4}$$

where c is the speed of light and $\lambda_0 = c/f_0$. In (4), the last two terms can be always ignored when $(N-1)\Delta f << f_0$ [12]. We then have its approximate expression as

$$r_{m,n}(t,\varphi,\theta,R) \approx \exp[\mathrm{j}2\pi f_{m,n}t - \mathrm{j}4\pi R/\lambda_0]\cdot \exp[\mathrm{j}4\pi(n-1)d\cos\theta\sin\varphi/\lambda_0]\cdot \exp[-\mathrm{j}4\pi(n-1)\Delta f R/c]\cdot \exp(-\mathrm{j}4\pi(m-1)d\sin\theta/\lambda_0). \quad (5)$$

Taking the narrowband assumption, the array vertical steering vector $\boldsymbol{\alpha}_{s\_v}(\theta)$ and horizontal steering vector $\boldsymbol{\alpha}_{s\_h}(\varphi,\theta,R)$ can be defined as

$$\boldsymbol{\alpha}_{s\_v}(\theta) = \exp[(-\mathrm{j}4\pi d\sin\theta/\lambda_0)(0:M-1)^{\mathrm{T}}]. \quad (6)$$

$$\boldsymbol{\alpha}_{s\_h}(\varphi,\theta,R) = \boldsymbol{\alpha}_{s\_h,\theta}(\varphi,\theta)\odot\boldsymbol{\alpha}_{s\_h,r}(R) = \exp[(\mathrm{j}4\pi d\cos\theta\sin\varphi/\lambda_0)(0:N-1)^{\mathrm{T}}]\odot \exp[(-\mathrm{j}4\pi\Delta f R/c)(0:N-1)^{\mathrm{T}}] \quad (7)$$

where $\odot$ denotes the Hadamard product. When the amplitude weights are all equal to one, the FDA two-way pattern steered to azimuth angle φ_0 and elevation angle θ_0 (or range R_0) is given by

$$p(t,\varphi,\theta,R) = \sum_{m=1}^{M}\sum_{n=1}^{N} r_{m,n}(t,\varphi,\theta,R)\cdot\exp[-\mathrm{j}4\pi(n-1)d\cos\theta_0\sin\varphi_0/\lambda_0]\cdot\exp[\mathrm{j}4\pi(n-1)\Delta f R_0/c]\cdot$$

$$\exp[\mathrm{j}4\pi(m-1)d\sin\theta_0/\lambda_0] = \sum_{m=1}^{M}\sum_{n=1}^{N}\exp[\mathrm{j}2\pi f_0(t-2R/c)]\cdot\exp[\mathrm{j}4\pi(n-1)d(\cos\theta\sin\varphi-\cos\theta_0\sin\varphi_0)/\lambda_0]\cdot$$

$$\exp[-\mathrm{j}4\pi(m-1)d(\sin\theta-\sin\theta_0)/\lambda_0]\cdot\exp[\mathrm{j}2\pi(n-1)\Delta f(t-2(R-R_0)/c)] =$$

$$\exp(\mathrm{j}\eta)\frac{\sin[-2M\pi d(\sin\theta-\sin\theta_0)/\lambda_0]}{\sin[-2\pi d(\sin\theta-\sin\theta_0)/\lambda_0]}\cdot\frac{\sin[2N\pi d(\cos\theta\sin\varphi-\cos\theta_0\sin\varphi_0)/\lambda_0+N\pi\Delta f(t-2(R-R_0)/c)]}{\sin[2\pi d(\cos\theta\sin\varphi-\cos\theta_0\sin\varphi_0)/\lambda_0+\pi\Delta f(t-2(R-R_0)/c)]} \quad (8)$$

where η is

$$\eta = 2\pi f_0(t-2R/c)+(N-1)\pi d\cos\theta\sin\varphi/\lambda_0-(N-1)\pi d\cos\theta_0\sin\varphi_0/\lambda_0-(N-1)\pi\Delta f(R-R_0)/c-(M-1)\pi d(\sin\theta-\sin\theta_0)/\lambda_0. \quad (9)$$

The absolute value of $p(t,\varphi,\theta,R)$ can be expressed as

$$|p(t,\varphi,\theta,R)| = \left|\frac{\sin[-2M\pi d(\sin\theta-\sin\theta_0)/\lambda_0]}{\sin[-2\pi d(\sin\theta-\sin\theta_0)/\lambda_0]}\right|\cdot \left|\frac{\sin[2N\pi d(\cos\theta\sin\varphi-\cos\theta_0\sin\varphi_0)/\lambda_0+N\pi\Delta f[t-2(R-R_0)/c)]}{\sin[2\pi d(\cos\theta\sin\varphi-\cos\theta_0\sin\varphi_0)/\lambda_0+\pi\Delta f(t-2(R-R_0)/c)]}\right|. \quad (10)$$

Note that $|p(t,\varphi,\theta,R)|$ is the product of two terms. The first term denotes the elevation pattern that is similar to the one in the conventional phased-array. While the second term is the function of not only spatial angles, but also range and time. This indicates that the FDA pattern is a time or range variant. In actual situations, we can fix the time in every scanning period, e.g. $t = 0$. Then, if the interested range is given, the time delay will be a constant and the pattern to the desired target position will also be fixed.

Furthermore, it is worth noticing that the element spacing d in (10) should be restricted to avoid grating boles in spatial angles. For the vertical elements of the array, it should satisfy

$$|2\pi d(\sin\theta-\sin\theta_0)/\lambda_0| \leqslant \pi. \quad (11)$$

The element spacing d can then be constrained to

$$d \leqslant \lambda_0/2\max[|\sin\theta-\sin\theta_0|] \quad (12)$$

where $\max[\cdot]$ denotes the maximum value of $[\cdot]$.

Similarly, the spacing for the horizontal elements of the array should satisfy

$$d \leqslant \lambda_0/[2\max(|\cos\theta\sin\varphi-\cos\theta_0\sin\varphi_0|)]. \quad (13)$$

Combining with (12) and (13), the constraint on the element spacing d for the FDA can be expressed as

$$d \leqslant \lambda_0/[2\max(|\sin\theta-\sin\theta_0|, |\cos\theta\sin\varphi-\cos\theta_0\sin\varphi_0|)]. \quad (14)$$

Assume we are required to scan from $0^\circ \leqslant \theta \leqslant 90^\circ$ and $-90^\circ \leqslant \varphi \leqslant 90^\circ$, then (14) becomes

$$d \leqslant \lambda_0/4. \quad (15)$$

2.2 STAP signal model for FDA radar

In this section, we present the STAP signal model of the FDA. During each coherent processing interval (CPI), a burst of K pulses are transmitted with a fixed PRF. The clutter Doppler frequency corresponding to $f_{m,n}$ is given by

$$f_{d_{m,n}} = 2v\cos\theta\cos\varphi f_{m,n}/c = 2v\cos\psi f_{m,n}/c \tag{16}$$

where $\cos\psi = \cos\theta\cos\varphi$. Then, the Doppler phase of the signal received by the (m,n)th element at the kth pulse can be expressed as

$$\begin{aligned}\varsigma_{m,n,k}(\varphi,\theta,v) &= 2\pi f_{d_{m,n}}(k-1)/f_r = \\ &4\pi v\cos\theta\cos\varphi(k-1)f_{m,n}/cf_r = \\ &4\pi v\cos\theta\cos\varphi(k-1)/\lambda_0 f_r + \\ &4\pi v\cos\theta\cos\varphi(k-1)(n-1)\Delta f/cf_r\end{aligned} \tag{17}$$

where f_r denotes the PRF. Similar to (4), by ignoring the second term, we have

$$\varsigma_{m,n,k}(\varphi,\theta,v) \approx 4\pi v\cos\theta\cos\varphi(k-1)/\lambda_0 f_r. \tag{18}$$

The clutter Doppler frequency can then be simplified as

$$f_{d_{m,n}} \approx f_d = 2v\cos\theta\cos\varphi/\lambda_0 \tag{19}$$

which is identical with that in the conventional phased-array. Consequently, the Doppler steering vector $\boldsymbol{\alpha}_t(\varphi,\theta,v)$ can be given by

$$\boldsymbol{\alpha}_t(\varphi,\theta,v) = \exp[(\mathrm{j}4\pi v\cos\theta\cos\varphi/\lambda_0 f_r)(0:K-1)^{\mathrm{T}}]. \tag{20}$$

Combining with (6), (7) and (20), the $MNK\times 1$ space-time steering vector in the FDA is

$$\boldsymbol{\alpha}(\varphi,\theta,R,v) = \boldsymbol{\alpha}_t(\varphi,\theta,v)\otimes\boldsymbol{\alpha}_{s\_h}(\varphi,\theta,R)\otimes\boldsymbol{\alpha}_{s\_v}(\theta) \tag{21}$$

where $\otimes$ denotes the Kronecker product. Generally, except the 3D-STAP methods [23], an adaptive/nonadaptive elevation beamformer will be applied on the elevation data before the STAP filter [20–22]. We then define the $NK\times 1$ space-time steering vector as

$$\overline{\boldsymbol{\alpha}}(\varphi,\theta,R,v) = \boldsymbol{\alpha}_t(\varphi,\theta,v)\otimes\boldsymbol{\alpha}_{s\_h}(\varphi,\theta,R). \tag{22}$$

According to the general clutter model introduced in [22], the clutter data from one range ring can be modeled as the superposition of N_c independent clutter patches evenly distributed in azimuth. When the range-ambiguous clutter contributes to the data, the $NK\times 1$ clutter data $\boldsymbol{c}$ can be expressed as

$$\boldsymbol{c} = \sum_{i=1}^{N_r}\sum_{j=1}^{N_c}\sigma_{ij}\overline{\boldsymbol{\alpha}}(\varphi_{ij},\theta_i,R_i,v) \tag{23}$$

where N_r is the number of range ambiguities. σ_{ij}, φ_{ij} and θ_i are the complex amplitude, the azimuth angle and the elevation angle of the ith ambiguous range, the jth clutter patch, respectively. Generally, the complex amplitudes from different patches and different ranges are assumed uncorrelated [9]. Hence the true clutter covariance matrix can be defined as

$$\boldsymbol{R}_c = \mathrm{E}[\boldsymbol{c}\boldsymbol{c}^{\mathrm{H}}] = \sum_{i=1}^{N_r}\sum_{j=1}^{N_c}|\sigma_{ij}|^2\overline{\boldsymbol{\alpha}}(\varphi_{ij},\theta_i,R_i,v)\overline{\boldsymbol{\alpha}}^{\mathrm{H}}(\varphi_{ij},\theta_i,R_i,v) \tag{24}$$

where $\mathrm{E}[\cdot]$ denotes the statistical expectation operator.

Assume the target is in the i_tth ambiguous range. σ_t, φ_t and θ_t are the target complex amplitude, the azimuth angle and the elevation angle, respectively. v_t is the relative velocity between the target and the platform. The target data $\boldsymbol{s}$ can be written as

$$\boldsymbol{s} = \sigma_t\overline{\boldsymbol{\alpha}}_t(\varphi_t,\theta_t,R_{i_t},v_t) = \sigma_t\boldsymbol{\alpha}_{t\_t}(v_t)\otimes\boldsymbol{\alpha}_{s\_h}(\varphi_t,\theta_t,R_{i_t}) \tag{25}$$

where $\overline{\boldsymbol{\alpha}}_t(\varphi_t,\theta_t,R_{i_t},v_t)$ denotes the target steering vector and $\boldsymbol{\alpha}_{t\_t}(v_t)$ denotes the target Doppler steering vector

$$\boldsymbol{\alpha}_{t\_t}(v_t) = \exp[(\mathrm{j}4\pi v_t/\lambda_0 f_r)(0:K-1)^{\mathrm{T}}]. \tag{26}$$

According to the minimum variance distortionless response (MVDR) criterion, the STAP weight vector can be calculated [3] by

$$\boldsymbol{w}_{\mathrm{opt}} = \frac{\boldsymbol{R}^{-1}\overline{\boldsymbol{\alpha}}_t(\varphi_t,\theta_t,R_{i_t},v_t)}{\overline{\boldsymbol{\alpha}}_t^{\mathrm{H}}(\varphi_t,\theta_t,R_{i_t},v_t)\boldsymbol{R}^{-1}\overline{\boldsymbol{\alpha}}_t(\varphi_t,\theta_t,R_{i_t},v_t)} \tag{27}$$

where $\boldsymbol{R}^{-1}$ denotes the inverse matrix of $\boldsymbol{R}$, and $\boldsymbol{R} = \boldsymbol{R}_c + \delta_n^2\boldsymbol{I}_{NK}$ is the clutter-plus-noise covariance matrix. δ_n^2 is the noise power. $\boldsymbol{I}_{NK}$ denotes the $NK\times NK$ identity matrix. In practice, the true covariance matrix $\boldsymbol{R}$ is not a known priori, and must be estimated from secondary range samples.

3. New characteristics of clutter in FDA radar

In this section, detailed discussions on the array beampattern and clutter distribution are presented, based on which the constraint on the frequency increment is designed.

Assume $t = 0$, we first compare the beampattern of the FDA with that of the conventional phased-array in Fig. 2, where the main parameters of the forward-looking airborne radar system are listed in Table 1. It is seen that the location of the mainlobe is changing at different ranges in the FDA.

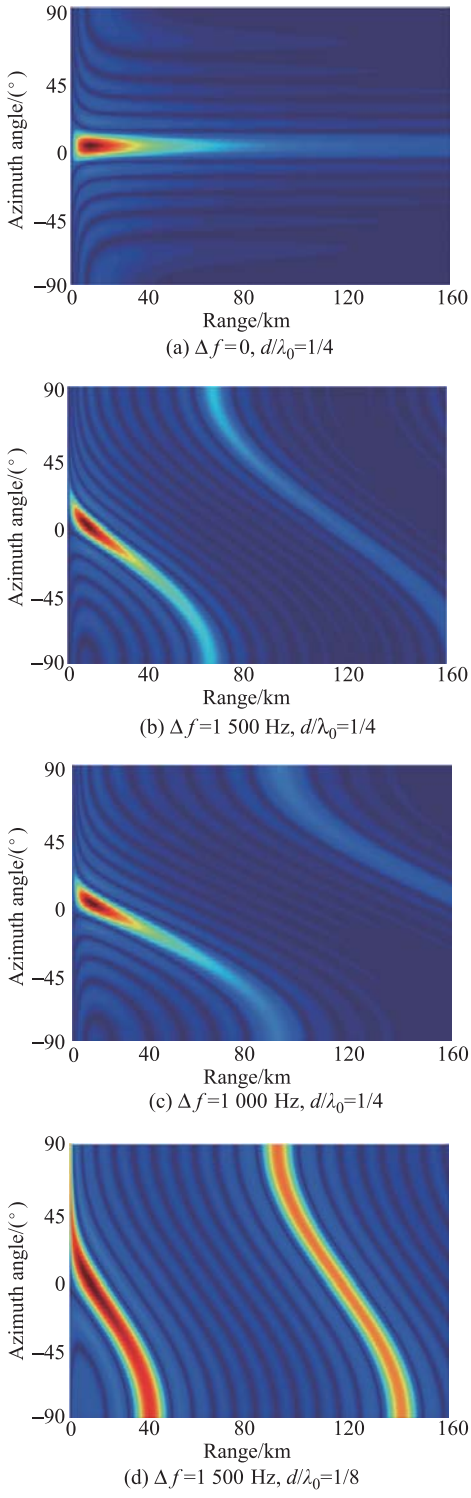

(a) Δf=0, d/λ_0=1/4

(b) Δf=1 500 Hz, d/λ_0=1/4

(c) Δf=1 000 Hz, d/λ_0=1/4

(d) Δf=1 500 Hz, d/λ_0=1/8

Fig. 2 Comparison of beampattern

Table 1 Parameters in forward-looking airborne radar

Parameter	Value
Carrier frequency/GHz	1
PRF/Hz	3 000
Platform velocity/(m/s)	180
Platform altitude/km	8
Bandwidth/MHz	10
Number of coherent pulses	16
Number of vertical elements	4
Number of horizontal elements	12
Azimuth angle of mainbeam center/(°)	0
Elevation angle of mainbeam center/(°)	30
Clutter to noise ratio (CNR)/dB	60

Based on (10), it can be also found that the grating lobes occur in the range dimension when

$$2\pi d(\cos\theta\sin\varphi - \cos\theta_0\sin\varphi_0)/\lambda_0 - 2\pi\Delta f(R - R_0)/c = a\cdot\pi. \tag{28}$$

or

$$R - R_0 = \frac{cd(\cos\theta\sin\varphi - \cos\theta_0\sin\varphi_0)}{\Delta f\lambda_0} - \frac{ac}{2\Delta f} \tag{29}$$

where a denotes the nonzero integer. For a uniform linear array, the grating lobes are spaced $c/2\Delta f$ from one another [13]. However, for a planar array, the distances of the grating lobes are not equal due to the coupling relationship between the range and the elevation angle. Specially, only when $\varphi = \varphi_0 = 0°$, we have

$$R - R_0 = -\frac{ac}{2\Delta f}. \tag{30}$$

From (29), we also find the pattern is a function of Δf and the ratio d/λ_0. As is shown in Fig. 2(c) and Fig. 2(d), the 'S'-shape of the pattern is increased when Δf decreases, while mitigated when d/λ_0 decreases. Note that the beamwidth of the mainlobe is inversely proportionate to the ratio of d/λ_0 [24], and the performance of the STAP method will degrade with the extended mainlobe clutter. Therefore, combining with (15), we consider the ratio $d/\lambda_0 = 1/4$ to avoid both the grating lobes and mainlobe widening in the spatial dimension. Further consideration on the design of the element spacing will not be undertaken in this paper.

With different values of Δf, Fig. 3 shows the ideal clutter spectrum under the assumption of the known covariance matrix. In this example, we set the number of range ambiguities $N_r = 2$. The reference range and ambiguous range are set to 16 km and 66 km, respectively. In Fig. 3(a), it is clearly shown that the clutter ridge locates in a semicircle, which agrees with the fact seen frequently in the conventional phased-array. While in Figs. 3(b), (c) and

(d), we see the Doppler shift of mainlobe clutter as well as the shift of the clutter spectrum along the spatial dimension. And the separation between the two clutter ridges becomes larger with the increase of Δf. Based on (5), it can be calculated that the shifted phase between the ambiguous ranges R_i $(i = 1, \ldots, N_r, i \neq i_t)$ and the reference range R_{i_t} is

$$\Delta\phi_i = 4\pi\Delta f|R_i - R_{i_t}|/c = 4\pi\Delta f|i - i_t|R_{\rm m}/c \quad (31)$$

where $R_{\rm m}$ denotes the maximum unambiguous range. Substituting $R_{\rm m} = c/2f_r$ into (31), we have

$$\Delta\phi_i = 2\pi\Delta f|i - i_t|/f_r. \quad (32)$$

When $N_r = 2$, (32) becomes

$$\Delta\phi = 2\pi\Delta f/f_r. \quad (33)$$

To distinguish the reference range clutter from the range-ambiguous clutter, we should require

$$2\pi\Delta f/f_r \neq a \cdot 2\pi. \quad (34)$$

Specially, when $\Delta\phi = \pi$ or $\Delta f = f_r/2$, the largest shift will be obtained, as is shown in Fig. 3(d).

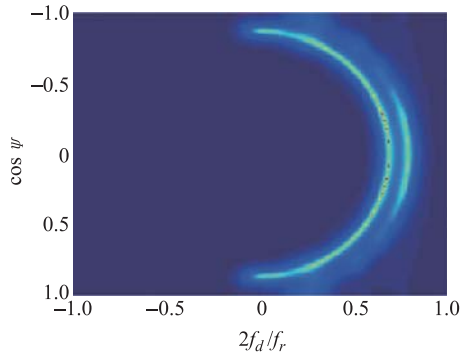

(a) Δf=0, d/λ_0=1/4

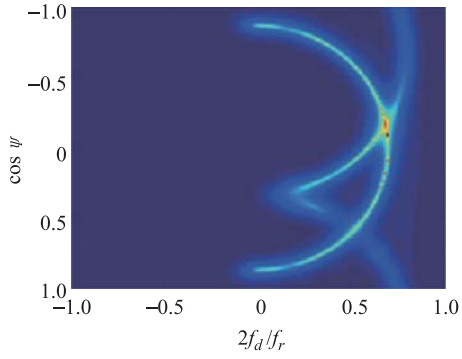

(b) Δf=1 000 Hz, d/λ_0=1/4

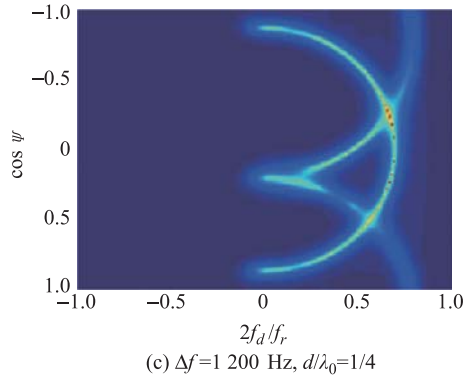

(c) Δf=1 200 Hz, d/λ_0=1/4

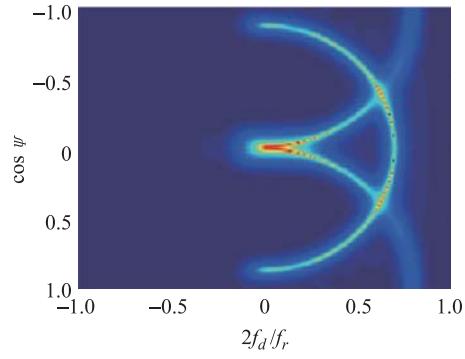

(d) Δf=1 500 Hz, d/λ_0=1/4

Fig. 3 Comparison of clutter spectrum with the true covariance matrix in forward-looking airborne radar

Practically, the number of range ambiguities is always larger than two for hypersonic vehicle-borne radar. Therefore, (34) should be rewritten as

$$2\pi\Delta f|i - i_t|/f_r \neq a \cdot 2\pi. \quad (35)$$

Combined with the definition of the FDA, it is reasonable to simplify (35) as

$$\Delta f|i - i_t|/f_r < 1. \quad (36)$$

Define $i_{\max} = \max|i - i_t|$, then we have

$$\Delta f < f_r/i_{\max} \quad (37)$$

which can be considered as the general constraint on the frequency increment to distinguish the range-ambiguous clutter.

In summary, FDA is different from the conventional phased-array in the clutter power distribution. It provides an additional DOF in range dimension and a potential mechanism to suppress the clutter at ambiguous ranges. When the number of range ambiguities is small, differences in clutter spectrum can be used directly to suppress the range-ambiguous clutter [19]. However, it cannot be applied to the hypersonic vehicle-borne radar, where the clutter at the reference range is indistinguishable from the range-ambiguous clutter in the space-time spectrum. To

solve this, the subspace projection algorithm is used to mitigate the range-ambiguous clutter in the FDA, which will be presented in the following sections.

4. Clutter suppression in FDA radar

Let x denote the $NK \times 1$ received data

$$\boldsymbol{x} = \boldsymbol{s} + \boldsymbol{c} + \boldsymbol{n} \tag{38}$$

where $\boldsymbol{n}$ is the noise data. It is worth noticing that the IID condition of secondary range samples is violated due to the range-dependent characteristic in the FDA. Even in range-unambiguous cases, STAP methods cannot be used directly. Therefore, a preparatory procedure should be adopted, where we consider a range compensating matrix as

$$\boldsymbol{T}^{(1)} = \mathrm{diag}[\boldsymbol{1}_K \otimes \boldsymbol{\alpha}^{\mathrm{H}}_{s\_h,r}(R_{i_t})] \tag{39}$$

where $\mathrm{diag}(\boldsymbol{q})$ denotes a diagonal matrix with its diagonal values given by the vector $\boldsymbol{q}$, and $\boldsymbol{1}_K$ denotes the $K \times 1$ all 1 vector. Then we have

$$\boldsymbol{x}^{(1)} = \boldsymbol{T}^{(1)}\boldsymbol{x}. \tag{40}$$

Specifically,

$$\begin{aligned}\boldsymbol{c}^{(1)} = \boldsymbol{T}^{(1)}\boldsymbol{c} = \sum_{j=1}^{N_c}\sigma_{i_tj}\overline{\boldsymbol{\alpha}}(\varphi_{i_tj},\theta_{i_t},0,v)+\\ \sum_{i=1,i\neq i_t}^{N_r}\sum_{j=1}^{N_c}\sigma_{ij}\overline{\boldsymbol{\alpha}}(\varphi_{ij},\theta_i,R_i-R_{i_t},v)=\\ \sum_{j=1}^{N_c}\sigma_{i_tj}\boldsymbol{\alpha}_t(\varphi_{i_tj},\theta_{i_t},v)\otimes\boldsymbol{\alpha}_{s\_h,\theta}(\varphi_{i_tj},\theta_{i_t})+\\ \sum_{i=1,i\neq i_t}^{N_r}\sum_{j=1}^{N_c}\sigma_{ij}\overline{\boldsymbol{\alpha}}(\varphi_{ij},\theta_i,(i-i_t)R_{\mathrm{m}},v)\end{aligned} \tag{41}$$

and

$$\begin{aligned}\boldsymbol{s}^{(1)} = \boldsymbol{T}^{(1)}\boldsymbol{s} = \sigma_t\overline{\boldsymbol{\alpha}}_t(\varphi_t,\theta_t,0,v_t) =\\ \sigma_t\boldsymbol{\alpha}_{t,t}(v_t)\otimes\boldsymbol{\alpha}_{s\_h,\theta}(\varphi_t,\theta_t).\end{aligned} \tag{42}$$

Note that the target data and the clutter in the reference range becomes range-independent after compensation while the clutter in ambiguous ranges remains range-dependent when Δf satisfies the constraint in (37).

After the compensation procedure, the subspace projection algorithm is developed for range-ambiguous clutter mitigation. Due to the serious ambiguity in range on the hypersonic platform, clutter in the conventional phased-array may have the same spatial and Doppler frequency from ambiguous ranges, resulting in the overlap of the clutter subspace and the suffering from the increased clutter power. However, with the additional DOF in range dimension, the FDA will be superior in separating the clutter subspace at the reference range from the ambiguous ranges. Based on the fact that the complex amplitudes have no effect on the accuracy of the clutter subspace [9], we construct the clutter subspace at the reference range as

$$\begin{aligned}\boldsymbol{P}_c = \sum_{j'=1}^{\widehat{N}_c}[\boldsymbol{\alpha}_t(\varphi_{i_tj'},\theta_{i_t},v)\otimes\boldsymbol{\alpha}_{s\_h,\theta}(\varphi_{i_tj'},\theta_{i_t})]\cdot\\ [\boldsymbol{\alpha}_t(\varphi_{i_tj'},\theta_{i_t},v)\otimes\boldsymbol{\alpha}_{s\_h,\theta}(\varphi_{i_tj'},\theta_{i_t})]^{\mathrm{H}}\end{aligned} \tag{43}$$

where $\widehat{N}_c$ denotes the clutter rank. In the side-looking case, it is known that the clutter rank [25] is given by the Brennan's rule

$$\widehat{N}_c = N + \beta(K-1) \tag{44}$$

where $\beta = 4v/f_r\lambda_0$ is an integer. In theory, the rank of the measurements depends on the observed time-bandwidth product, which is known as the Landau-Pollak theorem [26,27]. Applying the spatial bandwidth and the synthetic aperture to the Landau-Pollak theorem, the clutter rank in the forward-looking case can be approximated as

$$\widehat{N}_c = \mathrm{int}[2L/\lambda_0 + 4vT/\lambda_0 + 1] \tag{45}$$

where $\mathrm{int}(\cdot)$ denotes the nearest integer, $L = d(N-1)$ denotes the antenna aperture and $T = (K-1)/f_r$ denotes the coherent processing time.

Add the target subspace matrix $\boldsymbol{P}_s$, the subspace projection matrix can be expressed as

$$\boldsymbol{T}^{(2)} = \boldsymbol{P}_c + \boldsymbol{P}_s. \tag{46}$$

Generally, $\boldsymbol{P}_s$ is calculated by

$$\boldsymbol{P}_s = \overline{\boldsymbol{\alpha}}_t(\theta_t,\varphi_t,0,v_t)\overline{\boldsymbol{\alpha}}^{\mathrm{H}}_t(\theta_t,\varphi_t,0,v_t). \tag{47}$$

However, the value of v_t cannot be precisely known. To ensure the effectiveness and robustness of the proposed method, we can try to make use of the prior knowledge on desired targets, acquired either from a previous scanning or from other sensors. Assume the interested target velocity is restricted in $[v_1, v_2]$, $\boldsymbol{P}_s$ can be given by

$$\begin{aligned}\boldsymbol{P}_s = \sum_{q=0}^{N_q-1}\overline{\boldsymbol{\alpha}}_t(\theta_t,\varphi_t,0,(v_1+q\cdot\Delta v))\cdot\\ \overline{\boldsymbol{\alpha}}^{\mathrm{H}}_t(\theta_t,\varphi_t,0,(v_1+q\cdot\Delta v))\end{aligned} \tag{48}$$

where $N_q = \mathrm{int}[(v_2-v_1)/\Delta v] + 1$ and $\Delta v = f_r\lambda_0/2K$ denotes the velocity resolution. Then, we obtain

$$\boldsymbol{x}^{(2)} = \boldsymbol{T}^{(2)}\boldsymbol{x}^{(1)}. \tag{49}$$

After that, the method is provided for mitigating the range-dependence of the clutter spectrum, followed by the STAP filter to suppress the remaining clutter. To summarize, the clutter suppression based on the FDA technique

for hypersonic vehicle-borne radar (called method FDA-STAP for short) is implemented as follows:

Step 1 Elevation beamforming, which requires $O(MNK)$ flops;

Step 2 Use (39) to compensate the range phase, which requires $O(NK)$ flops;

Step 3 Use (46) to suppress the range-ambiguous clutter, which requires $O((\widehat{N}_c + N_q + 1)(NK)^2)$ flops;

Step 4 Mitigate the range-dependence of the clutter spectrum;

Step 5 STAP filtering.

To make a comparison, the computational complexities of range-ambiguous clutter mitigation between method FDA-STAP and the method of adaptive elevation beamforming [21] (called method AEB-STAP for short) are given. Considering the whole range cells, the computational complexities of the two methods are $O(LMNK + LNK + L(\widehat{N}_c + N_q + 1)(NK)^2)$ and $O(LMNK + 2LMN_r^2 + LN_r^3)$, respectively, where L is the number of the range cells. It can be observed that the number of range ambiguities is the main factor affecting the computational complexity of method AEB-STAP. While in method FDA-STAP, the computational complexity depends on both the clutter rank and DOF in the spatial and Doppler domain. Generally, the number of N_r is smaller than that of $\widehat{N}_c$ and NK. In this case, method FDA-STAP has a higher computational complexity than AEB-STAP.

5. Simulation results

In this section, we present numerical simulations to validate the effectiveness of the proposed method. The parameters of the simulated system are given in Table 2.

Table 2 Parameters in hypersonic vehicle-borne forward-looking radar

Parameter	Value
Carrier frequency/GHz	10
Platform velocity/(m/s)	1 700
Platform altitude/km	30
Bandwidth/MHz	10
Number of coherent pulses	32
Number of vertical elements	8
Number of horizontal elements	16
Element spacing/m	0.007 5
Azimuth angle of mainbeam center/(°)	0
Elevation angle of mainbeam center/(°)	30
Maximum range/km	100
Range of interested target velocity/(m/s)	[0,30]
CNR/dB	60

A moving target is set with an azimuth angel of 0° and a location of 60 km, whose relative velocity is set to 15 m/s. The additive noise is modeled as a complex Gaussian zero-mean spatially and temporally white random sequence. The signal-to-noise ratio (SNR) at per element and per pulse is 10 dB.

5.1 Example 1: clutter spectrum analysis in hypersonic vehicle-borne radar

With the known clutter covariance matrix, Fig. 4 shows the ideal clutter spectrum at 60 km. The corresponding eigenspectrum is shown in Fig. 5. It can be seen that the spectrum is seriously folded in the Doppler dimension due to the presence of Doppler ambiguities. As f_r increases, the effect is mitigated and the number of the bigger eigenvalues also decreases.

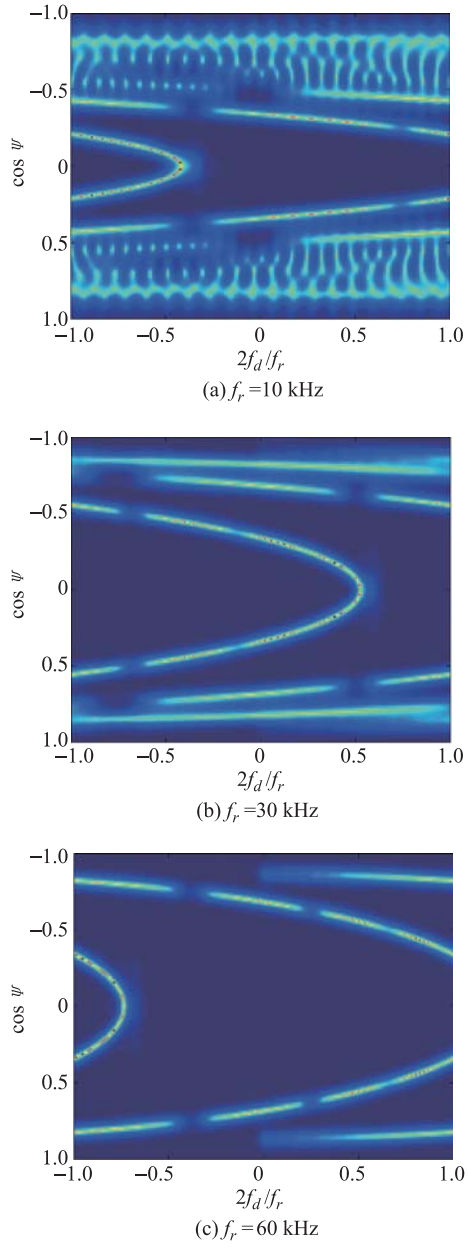

Fig. 4 Comparison of clutter spectrum with the true covariance matrix in the hypersonic vehicle-borne radar

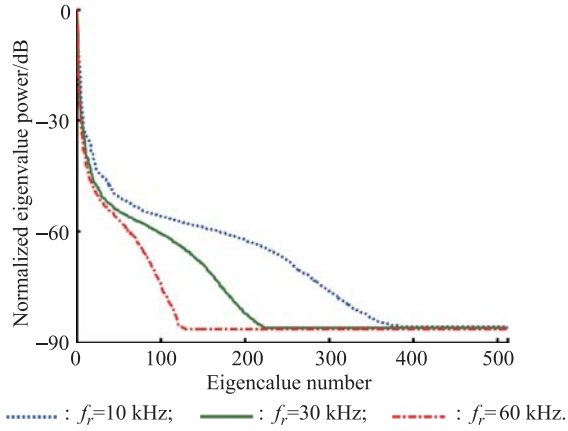

Fig. 5 Clutter eigenspectrum at $\Delta f = 0$

However, this would aggravate the range ambiguities. Therefore, a medium value of f_r is more appreciated in the hypersonic vehicle-borne radar systems to trade-off the range and Doppler ambiguities. Fig. 6 shows the eigenspectrum of the clutter covariance matrix with different values of Δf when $f_r = 30$ kHz. It can be seen that the numbers of the bigger eigenvalues are almost the same, which validates that the frequency increment has no influence on the clutter rank.

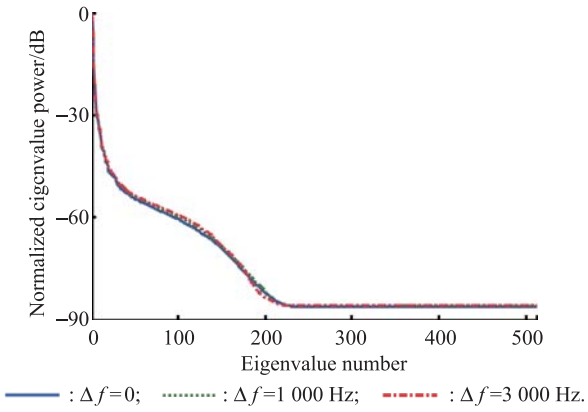

Fig. 6 Clutter eigenspectrum at $f_r = 30$ kHz

When the covariance matrix is estimated by the secondary range samples, the clutter spectrum is shown in Fig. 7. It is calculated that $i_{\max} \approx 8$ by the maximum range given in Table 2. Therefore, the value of Δf should be restricted in $(0, 3\,750\ \text{Hz})$. It can be seen that the spectrum in Fig. 7(a) is seriously widened in the Doppler dimension compared with that in Fig. 4(b). This is due to the increased range-ambiguous clutter and the effect of range-dependence with the forward-looking array. From Figs. 7(b) and (c), it can be also seen that the spectrums are irregularly distributed in both the spatial and Doppler dimension, which is caused by the arbitrary shifts from different range samples.

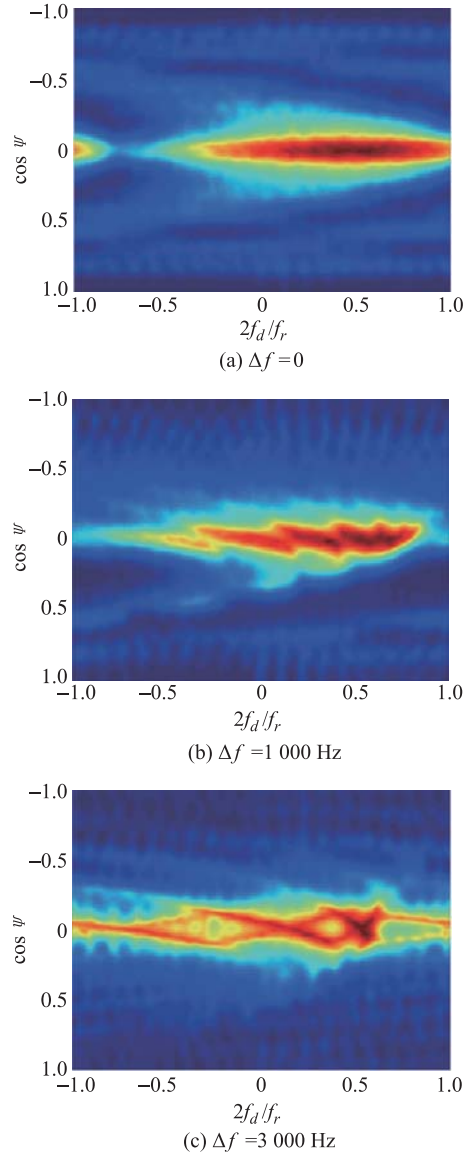

Fig. 7 Comparison of clutter spectrum with the estimated covariance matrix in the hypersonic vehicle-borne radar

5.2 Example 2: clutter suppression and performance comparison

In this example, the performance of method FDA-STAP is examined. The DW method is chosen for the range-dependence compensation in Step 4 [6]. Fig. 8 compares the performance between FDA-STAP and AEB-STAP with variable values of M. The improvement factor (IF) is used to evaluate the method performance, which is defined [3] as

$$\text{IF} = \frac{\text{SCNR}_{\text{out}}}{\text{SCNR}_{\text{in}}} = \frac{\delta_n^2(\text{CNR}+1)|\boldsymbol{w}_{\text{opt}}^{\text{H}}\overline{\boldsymbol{\alpha}}_t|^2}{\boldsymbol{w}_{\text{opt}}^{\text{H}}\boldsymbol{R}^{-1}\boldsymbol{w}_{\text{opt}}} \tag{50}$$

where SCNR_{in} and SCNR_{out} denote the input signal-to-clutter plus noise ratio (SCNR) and the out SCNR, respectively.

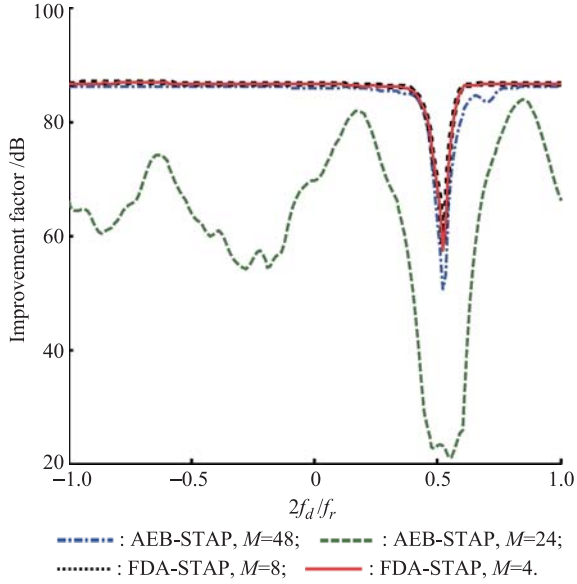

Fig. 8 Comparison of IF at $\Delta f = 3\,000$ Hz and $N = 16$

It is shown that FDA-STAP performs better than AEB-STAP even with smaller value of M. As M decreases, the IFs of FDA-STAP are almost invariable, which validates that the proposed method is independent from the elevation DOF. While the performance of AEB-STAP degrades greatly with the decrease of M due to the dependence of the elevation DOF. Besides, since the elevation angles of the ambiguous ranges are almost indistinguishable at a high platform altitude, more elevation DOF are required in AEB-STAP to null the range-ambiguous clutter completely. When $M = 48$ in the conventional phased-array and $M = 8$ in the FDA, Fig. 9 shows the performance of comparison with variable values of N.

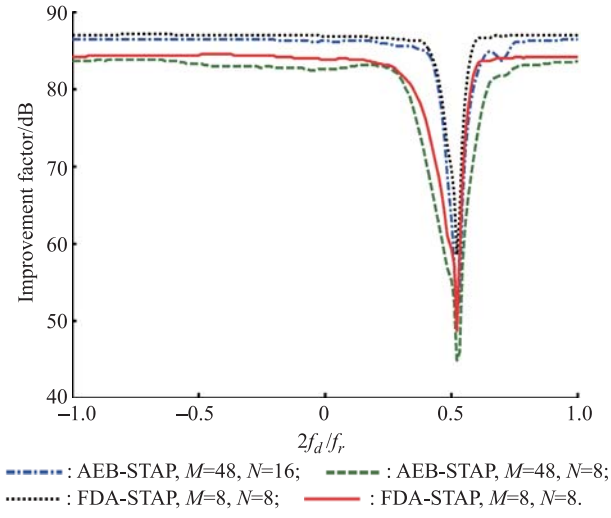

Fig. 9 Comparison of IF with variable values of N at $\Delta f = 3\,000$ Hz

Note that the notches of the two methods are all widened as N decreases. However, the performance of FDA-STAP is still better than that of AEB-STAP.

In the presence of amplitude and phase errors, Fig. 10 shows the performance of comparison where the amplitude error is assumed to obey the Gaussian distribution, and the phase error is assumed to obey the uniform distribution. It is noticed that the performance of AEB-STAP degrades as the array error increases, while the performance of FDA-STAP is almost unaffected, which verifies the robustness of the proposed method to the array error.

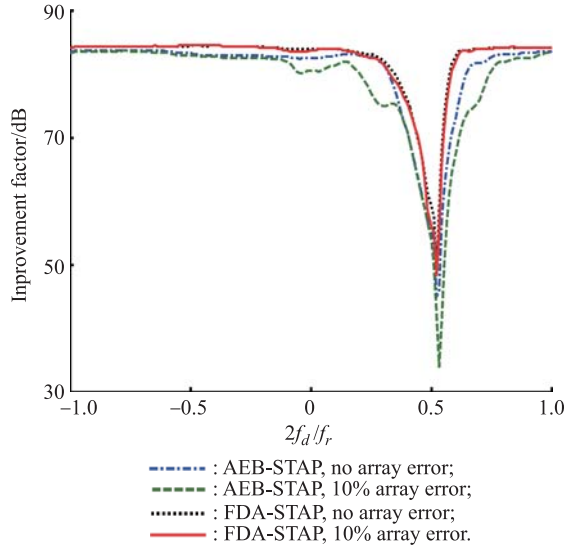

Fig. 10 Comparison of IF with amplitude and phase errors at $\Delta f = 3\,000$ Hz and $N = 8$

Finally, the IFs of FDA-STAP with variable values of Δf are shown in Fig. 11. Slight differences can be observed in the width of the notches. This means that the detection performance of the slowly moving target may be affected by the value of Δf.

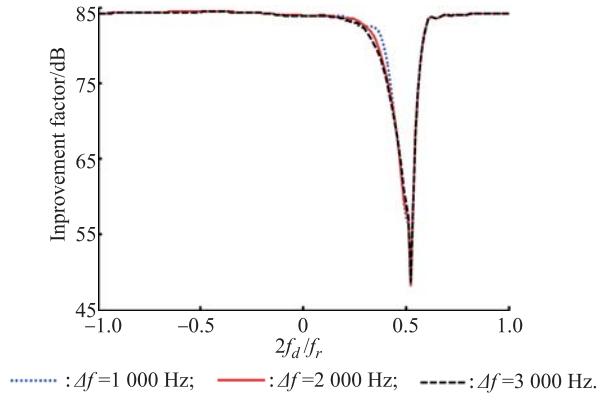

Fig. 11 Comparison of IF with variable values of Δf at $M = 8$ and $N = 8$

6. Conclusions

This paper presentes a new approach based on the FDA to suppress the clutter in hypersonic vehicle-borne radar. The essence is to utilize the range-dependent characteristic of the FDA to distinguish the clutter from ambiguous ranges, which is not accessible in the conventional phased-array. Based on the model of the FDA beampattern and STAP signal, the design of the FDA parameters is presented. For clutter suppression in hypersonic vehicle-borne radar, the seriously range-ambiguous clutter is mitigated by using the subspace projection algorithm. Simulation results verify that the proposed method performs better when the elevation DOF is limited. Its robustness to the array error is also examined by analyzing the IF.

However, there are also some problems to be considered further. First, the computational complexity of the proposed method is larger than that of the traditional method. Second, the vibration of the platform always exists in the practical situations. It would introduce the phase errors into the received signal, causing losses in SCNR and difficulties in target detection [28,29]. Therefore, the algorithms for motion compensation and clutter suppression with good efficiency and robustness will be studied in next work.

References

[1] R. L. Moses, V. L. Rausch, L. T. Nguyen. NASA hypersonic flight demonstrators-overview, status and future plans. Hampton, VA, USA: NASA Langley Research Center, 2004: 619 – 630.

[2] J. Hank, J. Murphy, R. Mutzman. The X-51A scramjet engine flight demonstration program. *Proc. of the AIAA International Space Planes and Hypersonic Systems and Technologies Conference*, 2008: 1 – 4.

[3] R. Klemm. *Applications of space-time adaptive processing*. London: Springer, 2004.

[4] R. Klemm. Adaptive airborne MTI: comparison of sideways and forward looking radar. *Proc. of the IEEE International Radar Conference*, 1995: 614 – 618.

[5] Z. Liu, Y. Chen, R. Xie, et al. Clutter property analysis and clutter suppression for hypersonic airborne radar. *Proc. of the International Conference on Radar*, 2013: 374 – 379.

[6] O. Kreyenkamp, R. Klemm. Doppler compensation in forward looking STAP radar. *IEE Radar, Sonar and Navigation*, 2001, 148(5): 253 – 258.

[7] M. Zatman. Circular array STAP. *IEEE Trans. on Aerospace and Electronic Systems*, 2000, 36(2): 510 – 517.

[8] F. D. Lapierre, M. V. Droogenbroeck, J. G. Verly. New methods for handling the range dependence of the clutter spectrum in non-sidelooking monostatic STAP radar. *Proc. of the IEEE International Conference on Acoustics, Speech, and Signal Processing*, 2003: 73 – 76.

[9] X. P. Yang, Y. X. Liu, T. Long. Geometry-aided subspace projection for mitigating range-dependence of the clutter spectrum in forward-looking airborne radar. *Proc. of the IEEE International Geoscience and Remote Sensing Symposium*, 2012: 6138 – 6141.

[10] P. Antonik, M. C. Wicks, H. D. Griffiths, et al. Frequency diverse array radars. *Proc. of the IEEE Radar Conference*, 2006: 215 – 217.

[11] J. J. Huang, K. F. Tong, C. J. Baker. Frequency diverse array with beam scanning feature. *Proc. of the IEEE Antennas and Propagation Society International Symposium*, 2008: 1 – 4.

[12] W. Q. Wang. Frequency diverse array antenna: new opportunities. *IEEE Antennas and Propagation Magazine*, 2015, 57(2): 145 – 152.

[13] P. F. Sammartino, C. J. Baker, H. D. Griffiths. Frequency diverse MIMO techniques for radar. *IEEE Trans. on Aerospace and Electronic Systems*, 2013, 49(1): 201 – 222.

[14] W. Q. Wang. Range-angle dependent transmit beampattern synthesis for linear frequency diverse arrays. *IEEE Trans. on Antennas and Propagation*, 2013, 61(8): 4073 – 4081.

[15] W. Q. Wang, H. C. So. Transmit subaperturing for range and angle estimation in frequency diverse array radar. *IEEE Trans. on Signal Processing*, 2014, 62(8): 2000 – 2011.

[16] J. Farooq, M. A. Temple, M. A. Saville. Application of frequency diverse arrays to synthetic aperture radar imaging. *Proc. of the International Conference on Electromagnetics in Advanced Applications*, 2007: 447 – 449.

[17] J. Farooq, M. A. Temple, M. A. Saville. Exploiting frequency diverse array processing to improve SAR image resolution. *Proc. of the IEEE Radar Conference*, 2008: 1 – 5.

[18] J. W. Xu, S. Q. Zhu, G. S. Liao. Space-time-range adaptive processing for airborne radar systems. *IEEE Sensors Journal*, 2014, 15(3): 1602 – 1610.

[19] P. Baizert, T. B. Hale, M. A. Temple, et al. Forward-looking radar GMTI benefits using a linear frequency diverse array. *Electronics Letters*, 2006, 42(22): 1311 – 1312.

[20] D. Wilcox, M. Sellathurai. Transmit beamforming for range ambiguous clutter mitigation in forward-looking STAP radar. *Sensor Signal Processing for Defence*, London, UK, 2011: 1 – 4.

[21] X. D. Meng, T. Wang, J. X. Wu, et al. Short-range clutter suppression for airborne radar by utilizing prefiltering in elevation. *IEEE Geoscience and Remote Sensing Letters*, 2009, 6(2): 268 – 272.

[22] J. X. Wu, T. Wang, X. D. Meng, et al. Clutter suppression for airborne non-sidelooking radar using ERCB-STAP algorithm. *IET Radar, Sonar and Navigation*, 2010, 4(4): 497 – 506.

[23] P. M. Corbell, T. B. Hale. 3-Dimensional STAP performance analysis using the cross-spectral metric. *Proc. of the IEEE Radar Conference*, 2004: 610 – 615.

[24] H. L. Van Trees. *Optimum array processing*. New York: Wiley, 2002.

[25] J. R. Guerci. *Space-time adaptive processing for radar*. London: Artech House, 2003.

[26] H. J. Landau, H. O. Pollak. Prolate spheroidal wave functions, fourier analysis and uncertainty-III: the dimension of the space of essentially time-and band-limited signals. *The Bell System Technical Journal*, 1962, 41(4): 1295 – 1336.

[27] N. A. Goodman, J. M. Stiles. On clutter rank observed by arbitrary arrays. *IEEE Trans. on Signal Processing*, 2007, 55(1): 178 – 186.

[28] G. Fornaro. Trajectory deviations in airborne SAR: analysis and compensation. *IEEE Trans. on Aerospace and Electronic Systems*, 1999, 35(3): 997 – 1009.

[29] U. Yilmaz. Effects of vibration on coherent homodyne radars. *Proc. of the IET International Radar Conference*, 2015: 1 – 7.

Biographies

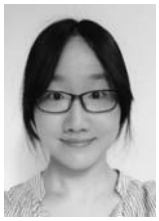

Xuzi Wu was born in 1989. She is a doctor postgraduate of National Key Laboratory of Radar Signal Processing in Xidian University, Xi'an, China. Her main research interest is signal processing and waveform design for cognitive radar system.
E-mail: wuxuzi1989@163.com

Zheng Liu was born in 1964. He is a professor, doctoral director and the vice director of National Key Laboratory of Radar Signal Processing in Xidian University, Xi'an, China. His main research interests include the theory and system design of radar signal processing, precision guiding technology and multi-sensor data fusion.
E-mail: lz@xidian.edu.cn

Rong Xie was born in 1982. He received his M.S. degree in signal and information processing and Ph.D. degree in pattern recognition and intelligent system from Xidian University, Xi'an, China, in 2006 and 2011, respectively. He is now an associate professor at National Key Laboratory of Radar Signal Processing. His main research interests include signal processing of MIMO radar, and array signal processing.
E-mail: rxie@mail.xidian.edu.cn